

Semantic-guided Masked Mutual Learning for Multi-modal Brain Tumor Segmentation with Arbitrary Missing Modalities

Guoyan Liang^{1*}, Qin Zhou^{2*}, Jingyuan Chen¹,
Bingcang Huang³, Kai Chen³, Lin Gu⁴, Zhe Wang^{2†}, Sai Wu^{1†}, Chang Yao^{1†}

¹Zhejiang University, Hangzhou, China

²Department of Computer Science and Engineering, ECUST, China

³Gongli Hospital of Shanghai Pudong New Area

⁴RIKEN AIP, The University of Tokyo

{guoyanl, jingyuanchen, wusai, changy}@zju.edu.cn, {sunniezq, wangzhe}@ecust.edu.cn

Abstract

Malignant brain tumors have become an aggressive and dangerous disease that leads to death worldwide. Multi-modal MRI data is crucial for accurate brain tumor segmentation, but missing modalities common in clinical practice can severely degrade the segmentation performance. While incomplete multi-modal learning methods attempt to address this, learning robust and discriminative features from arbitrary missing modalities remains challenging. To address this challenge, we propose a novel Semantic-guided Masked Mutual Learning (SMML) approach to distill robust and discriminative knowledge across diverse missing modality scenarios. Specifically, we propose a novel dual-branch masked mutual learning scheme guided by Hierarchical Consistency Constraints (HCC) to ensure multi-level consistency, thereby enhancing mutual learning in incomplete multi-modal scenarios. The HCC framework comprises a pixel-level constraint that selects and exchanges reliable knowledge to guide the mutual learning process. Additionally, it includes a feature-level constraint that uncovers robust inter-sample and inter-class relational knowledge within the latent feature space. To further enhance multi-modal learning from missing modality data, we integrate a refinement network into each student branch. This network leverages semantic priors from the Segment Anything Model (SAM) to provide supplementary information, effectively complementing the masked mutual learning strategy in capturing auxiliary discriminative knowledge. Extensive experiments on three challenging brain tumor segmentation datasets demonstrate that our method significantly improves performance over state-of-the-art methods in diverse missing modality settings.

Introduction

The accurate segmentation of brain tumors is crucial for clinical assessment and surgical planning (Bakas et al. 2017; Yan et al. 2020). In clinical practice, MRI scans across multiple imaging modalities, including T1-weighted (T1), contrast-enhanced T1-weighted (T1ce), T2-weighted (T2), and Fluid Attenuated Inversion Recovery (Flair) images,

are combined to enable accurate brain tumor segmentation. However, it is not uncommon for one or more modalities to be absent due to image corruption, artifacts, acquisition protocols, allergies to contrast agents, or cost constraints (Qiu et al. 2023). Recently, incomplete multi-modal brain tumor segmentation has been frequently studied to deal with various missing modality scenarios (Ding, Yu, and Yang 2021; Zhang et al. 2022; Liu et al. 2023). Despite significant advancements, it remains challenging to extract robust and discriminative multi-modal features when dealing with arbitrary missing modalities, which impacts segmentation performance.

Based on the assumption that brain tumor segmentation should yield consistent outcomes with the ground truth, irrespective of the modality combinations (e.g., T1+T2 or Flair+T2+T1ce) used for patient examination, we propose an innovative Semantic-guided Masked Mutual Learning (SMML) framework to integrate hierarchical consistency constraints along with auxiliary semantic priors from SAM, enhancing the robustness and discriminative ability of incomplete multi-modal learning. Our framework employs a masked dual-branch architecture to emulate a patient undergoing various examination scenarios with different missing modalities. Initially, full modality inputs are fed into both branches. We then randomly mask one or more modalities in each branch. The training process for each branch is supervised by the proposed hierarchical consistency constraints and the semantic prior derived from the SAM method.

To enhance the robustness of our dual-branch learning scheme with diverse missing modality inputs, we introduce hierarchical consistency constraints. These constraints operate on two levels: pixel-level and feature-level. The pixel-level bidirectional constraint enforces detailed consistency, ensuring that only reliable knowledge is exchanged during mutual learning. Simultaneously, to incorporate relational context into the distillation process, we leverage a feature-level constraint that explores the consistency of inter-sample and inter-class relationships between the two branches within the latent feature space.

To further improve the discriminative ability of each student branch, we introduce a semantic-guided refinement network. This network integrates auxiliary semantic informa-

*These authors contributed equally.

†Corresponding Authors.

tion from SAM with initial predictions to generate refined segmentation outputs. Notably, the refinement network is employed solely during training, imposing no additional computational burden during inference.

The overall contributions of our proposed method can be summarized as follows:

- We propose a novel SMML framework to learn robust and discriminative knowledge across various missing modality settings.
- We propose the hierarchical consistency constraints to enhance the robustness of the proposed SMML framework, where the pixel-level consistency selects and exchanges reliable knowledge across the dual branches, while the feature-level distillation guarantees the inter-sample and inter-class relational consistency.
- We introduce a refinement network that incorporates auxiliary semantic knowledge from the well-established SAM, thereby enhancing the discriminative ability of each branch without incurring any computational burden during inference.

Related Work

Multi-modal Brain Tumor Segmentation

Complete multi-modal learning has markedly improved the accuracy of brain tumor segmentation from MRI scans (Wang et al. 2022; Zhou et al. 2023; Shaker et al. 2024). (Han et al. 2020) design a trusted multi-view classifier to model the multi-modal uncertainties and fuse features via Dempster’s rule. (Wang et al. 2022) introduce an uncertainty-aware multi-modal learning model through cross-modal random network prediction.

However, practical scenarios often involve missing modalities due to image corruption, allergies to contrast agents, or cost constraints (Liu et al. 2023). Therefore, many efforts have been made to accommodate the practical scenarios of missing modalities. While some methods address diverse missing modality settings by training modality-specific models (Liu et al. 2021; Karimijafarbigloo et al. 2023), these approaches overlook the valuable complementary information present across modalities. Recent efforts have focused on effectively learning representative multi-modal features that can adapt flexibly to diverse missing modality scenarios. (Ding, Yu, and Yang 2021) introduce a region-aware fusion module (RFM) to enhance feature representation by considering the diverse sensitivities of different modalities to tumor regions. (Zhang et al. 2022) propose a transformer-based method that combines transformers and CNNs to learn modality-invariant representations.

Mutual Learning

Mutual Learning (ML) is a machine learning paradigm that involves the collaboration of multiple models to learn from each other. This collaborative learning process allows the models to improve their performance by sharing knowledge. Mutual learning approaches, grounded in knowledge distillation, can be broadly categorized into response-based, feature-based, and relation-based methods. Response-based

distillation (Hinton, Vinyals, and Dean 2015) involves matching the soft labels produced by multiple models. Feature-based distillation (Zagoruyko and Komodakis 2017; Huang and Wang 2017) focuses on aligning the pixel-wise or statistical feature distributions across different models, while relation-based distillation (Tung and Mori 2019; Wei, Luo, and Luo 2023) matches the sample relations.

Mutual learning has been increasingly applied in scenarios involving incomplete multi-modal data. (Li et al. 2021) propose to transfer the full-modal information from the teacher to guide the missing modality learning of the student branch. However, this approach necessitates a substantial volume of labeled full-modal data, which can be impractical to obtain in real-world applications. Besides, dense pixel-level or feature-level distillation may fail unexpectedly if one or more crucial modalities are absent during incomplete multi-modal learning. To address this, some methods (Yang et al. 2022; Wu et al. 2023) focus on distill the structured knowledge through the relation-based or graph-based methods. Despite notable advancements, there is a scarcity of mutual learning frameworks specifically designed to handle scenarios with arbitrary missing modality inputs. In this paper, we propose a novel semantic-guided masked mutual learning framework to enhance both the robustness and discriminative ability of mutual learning, thereby improving the performance of incomplete multi-modal learning with arbitrary missing modalities.

Method

To improve the robustness and discriminative power of incomplete multi-modal learning, we propose a novel Semantic-guided Masked Mutual Learning (SMML) framework. Given the full-modal inputs, we generate random modality dropout masks for each student branch and feed the resulting missing modality data into each branch to foster the learning of robust multi-modal knowledge. An overview of the proposed framework is depicted in Figure 1, which consists of two student branches. With diverse missing modality inputs, the dual-branch networks are supervised by Hierarchical Consistency Constraints (HCC) in addition to the classic segmentation loss. During training, each student branch is further guided by a Semantic-guided Refinement Network (SRN) to enhance the discriminative power of each branch. In SRN, semantic priors derived from SAM are combined with the initial predictions from each student branch to generate refined outputs, which are then used to supervise the training of each branch.

Semantic-guided Masked Mutual Learning

Assuming patients undergoing varied missing modality imaging protocols should yield consistent outcomes, we propose the Semantic-guided Masked Mutual Learning (SMML) framework with two parallel branches. Denote the number of modalities (Flair, T1ce, T1, and T2) as K , for each branch $i, i \in \{1, 2\}$, we introduce the modality-specific encoders $\psi_{e,i}^k(\cdot), i \in \{1, 2\}, k \in \{1, \dots, K\}$ to generate intermediate feature maps $\mathbf{F}_i^k \in \mathbb{R}^{H_i \times W_i \times Z_i \times d}$ for each modality input, where (H_i, W_i, Z_i) and d denote the spatial

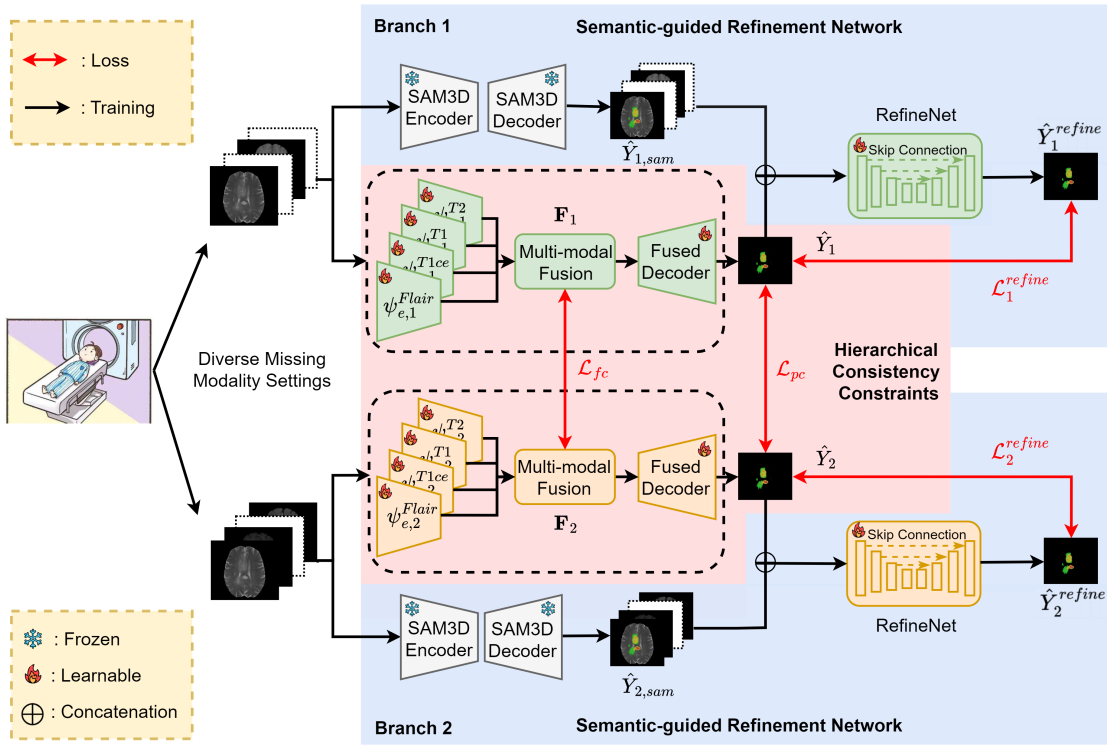


Figure 1: Overview of the proposed Semantic-guided Masked Mutual Learning (SMML) framework.

and channel dimensions of the intermediate feature maps.

For each branch i , given the complete multi-modal intermediate feature maps $\{\mathbf{F}_i^k, k \in \{1, \dots, K\}\}$, we obtain the simulated missing modality inputs by randomly masking out one or more modality features. Denote the random modality dropout mask for each branch as $M_i = \{M_i^k\}$, where each element is a binary value in $\{0, 1\}$, indicating the presence or absence of modality k in branch i . And $M_i^k = 0$ when the k -th modality of the i -th branch is missing, otherwise $M_i^k = 1$. Then the features of the missing modality k are substituted with zeros, while the features of the remaining modalities are left unchanged (i.e., $\mathbf{F}_i^k = \mathbf{F}_i^k * M_i^k$). The masked multi-modal feature set $\{\mathbf{F}_i^k, k \in 1, \dots, K\}$ are further processed by an attention-based multi-modal feature fusion module (Zhang et al. 2022) to generate the fused features $\mathbf{F}_1, \mathbf{F}_2 \in \mathbb{R}^{H_i \times W_i \times Z_i \times d_f}$ for each branch, where d_f is the fused feature dimension.

We then incorporate a fused decoder $\psi_{d,i}(\cdot)$ to generate the initial prediction for each branch as $\hat{Y}_i = \psi_{d,i}(\mathbf{F}_i)$. Each branch is further associated with a refinement network $f_i^{refine}(\cdot)$ to generate the refined segmentation predictions \hat{Y}_i^{refine} . The entire SMML framework is then supervised by the proposed Hierarchical Consistency Constraints and the Semantic-guided Refinement Network to enhance the robustness and discriminative ability of incomplete multi-modal learning with arbitrary missing modalities.

Hierarchical Consistency Constraints (HCC)

To leverage both detailed and relational context knowledge for robust learning, our HCC strategy involves consistency at both the pixel-level and the feature-level.

Pixel-level Bidirectional Constraint (PBC) Considering the sensitivity of different modalities to diverse tumor regions, the performance of each branch may suffer from severe performance degradation due to the absence of critical modality information. To improve the robustness of learning in the proposed SMML framework, we introduce pixel-level bidirectional distillation to selectively exchange reliable knowledge across the two branches.

With the initial predictions $\hat{Y}_1, \hat{Y}_2 \in \mathbb{R}^{H \times W \times Z \times C}$ from the two branches, where H, W, Z correspond to the spatial dimensions of the input image, and C is the number of classes. We proceed to compute the cross entropy loss between \hat{Y}_1, \hat{Y}_2 and the ground truth one hot segmentation map Y_{oh} as,

$$Q_1 = \sum_{c=1}^C -Y_{oh} \log(\sigma(\hat{Y}_1)), \quad (1)$$

$$Q_2 = \sum_{c=1}^C -Y_{oh} \log(\sigma(\hat{Y}_2)),$$

where $\sigma(\cdot)$ is the softmax operation. The pixel-wise cross entropy loss $Q_1, Q_2 \in \mathbb{R}^{H \times W \times Z}$ for each branch measure the deviation from the ground truth segmentation map. A lower loss value indicates a prediction that is more reliable. Therefore, we can obtain the bidirectional transfer mask $T_M \in \mathbb{R}^{H \times W \times Z}$ as,

$$T_M(h, w, z) = \mathbb{1}[Q_1(h, w, z) > Q_2(h, w, z)], \quad (2)$$

where $\mathbb{1}[\cdot]$ is the indicator function that evaluates to 1 when the inside condition is true, and 0 otherwise. $T_M(h, w, z)$ refers to the transferring direction at pixel (h, w, z) , and $T_M(h, w, z) = 1$ means the reliable knowledge is exchanged from branch 2 to branch 1.

The pixel-wise consistency loss for each branch is then calculated based on the transferring mask as,

$$\begin{aligned}\mathcal{L}_1^{pc} &= \frac{1}{N_{21}} \sum_{h,w,z} T_M * KL(\hat{Y}_1/\tau || \hat{Y}_2/\tau), \\ \mathcal{L}_2^{pc} &= \frac{1}{N_{12}} \sum_{h,w,z} (1 - T_M) * KL(\hat{Y}_2/\tau || \hat{Y}_1/\tau),\end{aligned}\quad (3)$$

where $N_{21} = \sum_{h,w,z=1}^{H,W,Z} T_M(h, w, z)$, $N_{12} = H * W * Z - N_{21}$. N_{21} denotes the number of pixels that facilitate the transfer of knowledge from branch 2 to branch 1, and vice versa for N_{12} . τ is the temperature hyper-parameter. The process ensures that knowledge is reliably exchanged across the students, improving the segmentation performance.

Feature-level Relational Constraint (FRC) Given that different branches should exhibit similar feature distributions, leveraging the feature affinity between inter-class prototypes (centers) is an effective strategy for robust relational context distillation in our masked mutual learning. As depicted in Figure 2, the FRC module comprises three key components: 1) a class-specific prototype generator, 2) a mechanism for generating inter-sample and inter-class relational context, and 3) an uncertainty-based re-weighting scheme to prioritize consistency learning from hard classes.

class-specific prototype generator: Given the fused features $\mathbf{F}_1, \mathbf{F}_2 \in \mathbb{R}^{H_i \times W_i \times Z_i \times d_f}$, and the corresponding segmentation mask $Y \in \mathbb{R}^{H \times W \times Z}$, we first interpolate Y into the same spatial dimension as $\mathbf{F}_1, \mathbf{F}_2$, then we can get the prototype $\mathbf{p}_1^c, \mathbf{p}_2^c$ for each semantic class c as,

$$\begin{aligned}\mathbf{p}_1^c &= \frac{1}{N_c} \sum_{h,w,z=1}^{H_i, W_i, Z_i} \mathbb{1}[Y(h, w, z) = c] * \mathbf{F}_1(h, w, z), \\ \mathbf{p}_2^c &= \frac{1}{N_c} \sum_{h,w,z=1}^{H_i, W_i, Z_i} \mathbb{1}[Y(h, w, z) = c] * \mathbf{F}_2(h, w, z),\end{aligned}\quad (4)$$

where N_c denotes the number of pixels belonging to class c .

inter-sample and inter-class relational context modeling: During the training of each mini-batch, denote the batchsize as B , the number of semantic classes as C , then according to Eq. 4, we can obtain the prototype of the c -th class in the b -th sample for each branch as $\mathbf{p}_1^{b,c}$ and $\mathbf{p}_2^{b,c}$, respectively. The inter-sample and inter-class relational context $R_1, R_2 \in \mathbb{R}^{(B*C) \times (B*C)}$ for each branch can be calculated as,

$$\begin{aligned}R_1(b_1, c_1; b_2, c_2) &= \frac{\langle \mathbf{p}_1^{b_1, c_1}, \mathbf{p}_1^{b_2, c_2} \rangle}{\|\mathbf{p}_1^{b_1, c_1}\|_2 \|\mathbf{p}_1^{b_2, c_2}\|_2}, \\ R_2(b_1, c_1; b_2, c_2) &= \frac{\langle \mathbf{p}_2^{b_1, c_1}, \mathbf{p}_2^{b_2, c_2} \rangle}{\|\mathbf{p}_2^{b_1, c_1}\|_2 \|\mathbf{p}_2^{b_2, c_2}\|_2},\end{aligned}\quad (5)$$

where \langle, \rangle calculates the dot product between two items, and $R_i(b_1, c_1; b_2, c_2)$ denotes the feature similarity between

the c_1 -th class of the b_1 -th sample and the c_2 -th class of the b_2 -th sample in branch i . The initial inter-sample and inter-class relational distance is calculated as,

$$D_r^{b_1, c_1} = \sum_{b_2, c_2=1}^{B, C} (R_1(b_1, c_1; b_2, c_2) - R_2(b_1, c_1; b_2, c_2))^2, \quad (6)$$

where $D_r^{b_1, c_1}$ is the overall relational difference between the c_1 -th class of the b_1 -th sample across the two branches.

uncertainty based re-weighting scheme: To prioritize consistency learning on more challenging classes, we introduce a re-weighting scheme based on class-specific uncertainty. With the initial predictions $\hat{Y}_1, \hat{Y}_2 \in \mathbb{R}^{H \times W \times Z \times C}$, we first get the normalized prediction scores using softmax as $\sigma(\hat{Y}_i), i \in \{1, 2\}$. Denote the normalized prediction scores of the c -th class as $\hat{Y}_i^c \in \mathbb{R}^{H \times W \times Z}$, then the class-specific weights $W_i = \{W_i^c\} \in \mathbb{R}^C$ are obtained as,

$$\begin{aligned}W_1^c &= \sum -\hat{Y}_1^c \log(\hat{Y}_1^c), \\ W_2^c &= \sum -\hat{Y}_2^c \log(\hat{Y}_2^c).\end{aligned}\quad (7)$$

The final uncertainty weights are the mean of weights from both branches,

$$W^c = (W_1^c + W_2^c)/2. \quad (8)$$

Similarly, we can calculate the class-specific weights for each sample within the mini-batch. Denote W^{b_1, c_1} as the weight for the c_1 -th class of the b_1 -th sample, the final feature-level relational consistency loss is calculated as,

$$\mathcal{L}_{fc} = \sum_{b_1, c_1=1}^{B, C} D_r^{b_1, c_1} * W^{b_1, c_1}. \quad (9)$$

Semantic-guided Refinement Network

To further enhance the discriminative power of our method, we propose incorporating auxiliary semantic cues from the well-established SAM model (Kirillov et al. 2023). While the SAM model has demonstrated impressive zero-shot segmentation capabilities in 2D natural images, its efficacy is significantly compromised when applied to medical images, primarily due to the lack of medical domain expertise. Consequently, we opt for the SAM-Med3D model (Wang et al. 2023), which has been specifically trained on a variety of 3D medical imaging tasks, to produce supplementary semantic segmentation cues.

For each branch i , with the initial segmentation predictions \hat{Y}_i , and the zero-shot segmentation results $\hat{Y}_{i, sam}^k$ generated from each modality k using SAM-Med3D, we first substitute the missing modality results with all zeros (i.e., $\hat{Y}_{i, sam}^k = 0 | M_i^k = 0$, where M_i^k refers to the previously defined random modality dropout mask), then the multi-modal semantic cues from SAM, denoted as $\hat{Y}_{i, sam} = \{\hat{Y}_{i, sam}^k, k \in 1, \dots, K\}$, are concatenated with the initial prediction along the channel dimension. The combined predictions are further fed forward through a refinement network to get the refined segmentation results,

$$\hat{Y}_i^{refine} = f_i^{refine}(Cat[\hat{Y}_{i, sam}, \hat{Y}_i]), \quad (10)$$

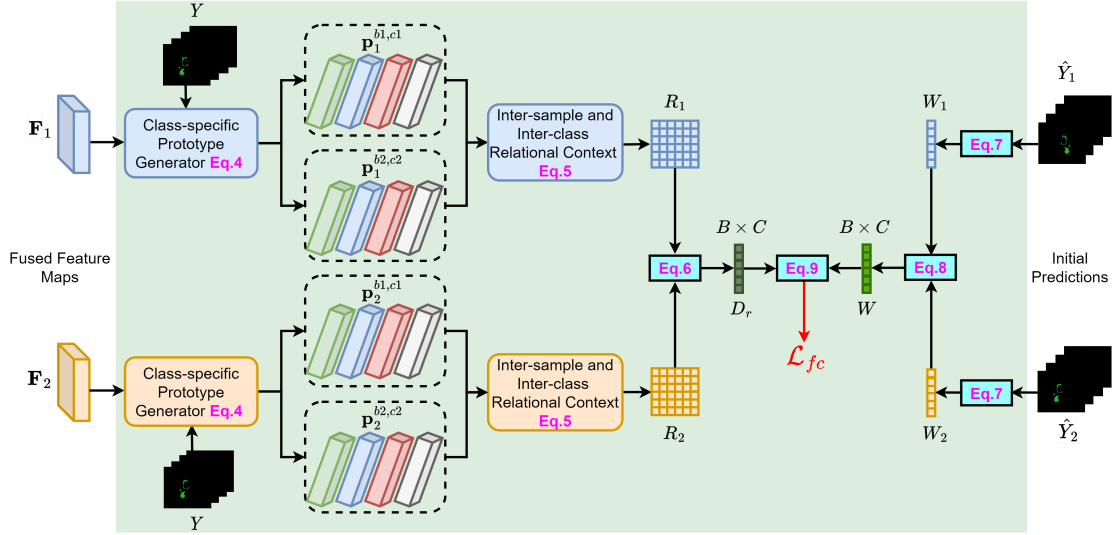


Figure 2: Illustration of the Feature-level Relational Constraint (FRC) module.

where $f_i^{refine}(\cdot)$ is the refinement network of branch i , which is a simple UNet model, $Cat[\cdot, \cdot]$ refers to concatenation along the channel dimension. The refined segmentation results are then utilized to guide the training by measuring the consistency between the initial and refined predictions,

$$\begin{aligned} L_1^{refine} &= KL(\hat{Y}_1 || \hat{Y}_1^{refine}), \\ L_2^{refine} &= KL(\hat{Y}_2 || \hat{Y}_2^{refine}). \end{aligned} \quad (11)$$

Please be aware that the refinement network operates solely during the training phase and does not impose any computational overhead during inference.

Training and Inference

Denote the classic segmentation loss on the initial predictions \hat{Y}_i and the refined predictions \hat{Y}_i^{refine} as,

$$\begin{aligned} L_1^{task} &= CE(\hat{Y}_1, Y) + Dice(\hat{Y}_1, Y), \\ L_2^{task} &= CE(\hat{Y}_2, Y) + Dice(\hat{Y}_2, Y), \\ L_{1,refine}^{task} &= CE(\hat{Y}_1^{refine}, Y) + Dice(\hat{Y}_1^{refine}, Y), \\ L_{2,refine}^{task} &= CE(\hat{Y}_2^{refine}, Y) + Dice(\hat{Y}_2^{refine}, Y), \end{aligned} \quad (12)$$

where $CE(\cdot)$, $Dice(\cdot)$ refer to the cross entropy and dice losses, respectively. Then the overall objectives of the proposed method for each branch is formulated as,

$$\begin{aligned} \mathcal{L}_1 &= \mathcal{L}_1^{task} + \mathcal{L}_{1,refine}^{task} + \mathcal{L}_1^{pc} + \mathcal{L}_{fc} + \mathcal{L}_1^{refine}, \\ \mathcal{L}_2 &= \mathcal{L}_2^{task} + \mathcal{L}_{2,refine}^{task} + \mathcal{L}_2^{pc} + \mathcal{L}_{fc} + \mathcal{L}_2^{refine}. \end{aligned} \quad (13)$$

The final loss objective for each branch, denoted as L_i , $i \in \{1, 2\}$, is used to guide the learning process of the respective branch during training.

During inference, to assess performance under each missing modality setting, we duplicate inputs with the arbitrary missing modalities and feed them to each branch to generate the initial predictions \hat{Y}_1 and \hat{Y}_2 . The final segmentation mask is predicted by taking the mean of \hat{Y}_1 and \hat{Y}_2 .

Experiments and Results

We demonstrate the effectiveness of our SMML framework through comprehensive comparison with state-of-the-art methods and an ablation study in the subsequent sections. Additionally, we validate its generalization capability with experiments on incomplete multi-modal segmentation of natural images, as detailed in the [supplementary material](#).

Datasets and Evaluation Metrics

The subjects in the BraTs 2018 and BraTs 2020 datasets (Menze et al. 2014) are categorized into four subregions: background, necrosis, edema, and enhancing tumor. In contrast, images in BraTs 2015 are divided into five subregions, which include the aforementioned categories plus an additional one for non-enhancing tumor. These subregions are further consolidated into three nested subregions: whole tumor, tumor core, and enhancing tumor. All volumetric data have been co-registered to a standard anatomical template and interpolated to a uniform resolution as provided by the dataset organizers.

Consistent with prior approaches (Ding, Yu, and Yang 2021; Liu et al. 2023), the BraTs 2015 dataset, comprising 274 subjects with public ground truth, is distributed into training, validation, and testing sets of 242, 12, and 20 samples, respectively. In the BraTs 2018 dataset, 285 annotated samples are allocated into training, validation, and testing sets of 199, 29, and 57, respectively. Likewise, BraTs 2020's labeled images are split into training, validation, and testing sets of 219, 50, and 100, respectively. The Dice Similarity Coefficient (DSC) is employed as the evaluation metric to assess the performance of brain tumor segmentation.

Implementation Details

All experiments were conducted using Python 3.9, PyTorch 2.1.1, and Ubuntu 22.04. The proposed SMML framework was trained on two NVIDIA A800 GPUs with 80GB of

M	Flair T1ce T1 T2	•	○	○	○	•	○	○	•	○	•	○	•	○	•	○	•	○	Avg
		○	○	•	○	○	•	○	•	○	○	•	○	•	○	•	○	•	
WT	MCTSeg	84.3	73.8	73.1	84.4	88.6	86.0	79.2	88.5	86.5	88.1	87.0	89.4	89.0	88.8	89.6	85.1		
	M3AE	88.7	75.8	74.4	84.8	89.7	86.7	77.2	89.9	86.3	89.0	85.7	90.2	89.9	88.9	90.6	85.8		
	U-Net-MFI	86.4	75.2	74.2	85.6	90.0	86.6	78.7	90.0	86.5	89.5	86.9	90.8	90.3	90.1	90.9	86.1		
	RFNet	84.4	74.9	73.6	84.8	88.4	86.6	78.4	88.6	86.8	87.8	87.2	89.5	89.2	88.9	89.6	85.3		
	mmFormer	85.7	77.9	76.5	86.0	88.7	86.8	80.4	88.7	86.9	88.1	87.1	89.7	89.1	89.0	89.7	86.0		
	SMU-Net	87.5	80.3	78.6	85.7	88.4	85.6	80.3	87.9	86.1	87.3	86.5	88.2	88.3	88.2	88.9	85.9		
Ours	87.9	79.8	78.7	87.0	89.5	87.6	82.8	89.9	87.6	89.7	87.9	89.9	89.7	90.3	89.9	87.2			
TC	MCTSeg	59.9	79.7	56.4	66.2	82.4	68.6	82.3	69.5	83.4	67.4	83.6	83.2	70.3	82.9	83.0	74.6		
	M3AE	66.4	82.9	66.1	69.4	84.4	71.8	83.4	70.9	84.2	70.8	84.4	84.6	72.7	84.1	84.5	77.4		
	U-Net-MFI	63.7	80.9	63.1	67.5	84.7	71.4	91.9	71.3	84.0	72.7	84.1	85.5	74.0	85.2	85.6	77.0		
	RFNet	63.5	79.9	61.1	65.7	81.9	71.1	81.2	70.8	83.1	71.5	83.9	83.4	72.8	83.2	84.0	75.8		
	mmFormer	62.9	81.9	62.1	69.7	82.7	69.6	82.8	71.3	83.4	68.7	83.9	83.3	70.6	83.5	83.9	76.0		
	SMU-Net	71.8	84.1	69.5	67.2	84.1	73.5	84.4	71.2	85.0	71.2	84.4	82.5	67.9	84.2	87.3	77.9		
Ours	67.7	83.1	65.4	71.7	84.8	73.6	84.0	73.4	84.8	72.9	84.9	86.3	74.9	84.7	85.2	78.5			
ET	MCTSeg	37.7	73.3	28.1	37.2	74.8	40.1	73.1	43.1	76.9	39.7	75.3	75.3	46.5	75.4	75.4	58.1		
	M3AE	35.6	73.7	37.1	47.6	75.0	48.7	74.7	45.4	75.3	41.2	75.4	73.8	44.8	74.0	75.5	59.9		
	U-Net-MFI	37.6	76.2	32.3	37.4	78.8	41.4	76.8	42.5	77.6	41.3	77.9	79.4	43.4	79.8	80.0	60.2		
	RFNet	34.7	70.0	30.2	40.8	71.6	42.7	72.8	44.9	72.3	39.5	74.5	73.5	46.1	74.1	74.3	57.5		
	mmFormer	39.0	75.3	37.7	45.8	76.0	45.0	78.1	44.5	77.8	43.2	78.5	77.6	46.3	79.2	79.4	61.5		
	SMU-Net	46.1	78.3	42.8	43.1	77.1	47.7	75.1	46.0	75.7	44.0	76.2	75.4	43.1	76.2	79.3	61.8		
Ours	41.0	79.1	39.4	47.8	81.8	45.2	79.9	46.5	81.6	45.1	81.6	81.5	48.9	81.5	81.7	64.2			

Table 1: Comparisons with the SOTA methods on the BraTs 2018 dataset. Performance is evaluated based on Dice Similarity Coefficient (DSC) scores for the whole tumor (WT), tumor core (TC), and enhancing tumor (ET). Hollow circles indicate the absence of that modality. The best results are highlighted in **bold**, while the second-best scores are indicated in **blue**.

memory. The Adam optimizer was used for model optimization, with β_1 and β_2 parameters set to 0.9 and 0.999 respectively, and a weight decay of $1e-4$. The ‘poly’ learning rate policy was adopted, starting with an initial learning rate of $2e-4$. The temperature hyper-parameter τ is empirically set to 6. During training, input images were randomly cropped to $128 \times 128 \times 128$ and then augmented using random flipping, cropping, and intensity shifts. The model was trained for 1000 epochs with a batch size of 2.

Methods	Avg DSC scores (%)			
	WT	TC	ET	Mean
MCTSeg	85.8	66.6	60.8	71.1
M3AE	85.6	67.6	59.7	71.0
U-Net-MFI	85.7	69.3	61.2	72.1
RFNet	85.4	71.1	63.0	73.2
mmFormer	86.9	71.7	62.4	73.7
SMU-Net	86.7	72.1	62.7	73.8
Ours	87.6	72.8	64.9	75.1

Table 2: Comparison results on the BraTs 2015 dataset.

Comparison with State-of-the-art Methods

We compare the proposed SMML with SOTA methods, including RFNet (Ding, Yu, and Yang 2021), mmFormer (Zhang et al. 2022), U-Net-MFI (Zhao, Yang, and Sun 2022), SMU-Net (Azad, Khosravi, and Merhof 2022), M3AE (Liu et al. 2023) and MCTSeg (Kang et al. 2024).

We evaluate our method on three challenging multi-modal brain tumor segmentation datasets. We record the de-

tailed results under different scenarios with arbitrary missing modality settings. The quantitative comparison results on the BraTs 2015, BraTs 2018, and BraTs 2020 datasets are presented in Table 1, Table 2, and Table 3, respectively. On BraTs 2018, we provide detailed comparison results for all missing modality settings. For BraTs 2015 and BraTs 2020, we report the average DSC scores across fifteen different missing modality combinations for brevity. MCTSeg, M3AE, U-Net-MFI, mmFormer, and SMU-Net were evaluated on only one or two datasets. For a thorough comparison, we replicated their results on the remaining datasets using the official implementations.

As shown in Tables 1, 2, and 3, our approach markedly improves segmentation accuracy, achieving state-of-the-art performance across all three datasets and tumor categories. Specifically, our SMML approach outperforms the second-best method with mean DSC score gains of 1.4% on BraTs 2018, 1.3% on BraTs 2015 and 1.7% on BraTs 2020, respectively. In the detailed comparison of scenarios with arbitrary missing modalities (as shown in Table 1), our proposed SMML achieves the highest or runner-up DSC scores in the majority of missing modality configurations across the three semantic categories.

Figure 3 displays qualitative comparison results, featuring two samples from the BraTs 2018 dataset. The comparison demonstrates that our method accurately identifies the tumor locations and covers the majority of tumor regions in different modal combination scenarios, while previous methods exhibit incomplete or incorrect tumor delineation. Furthermore, we note that previous methods exhibit suboptimal segmentation performance when only a single Flair or T1

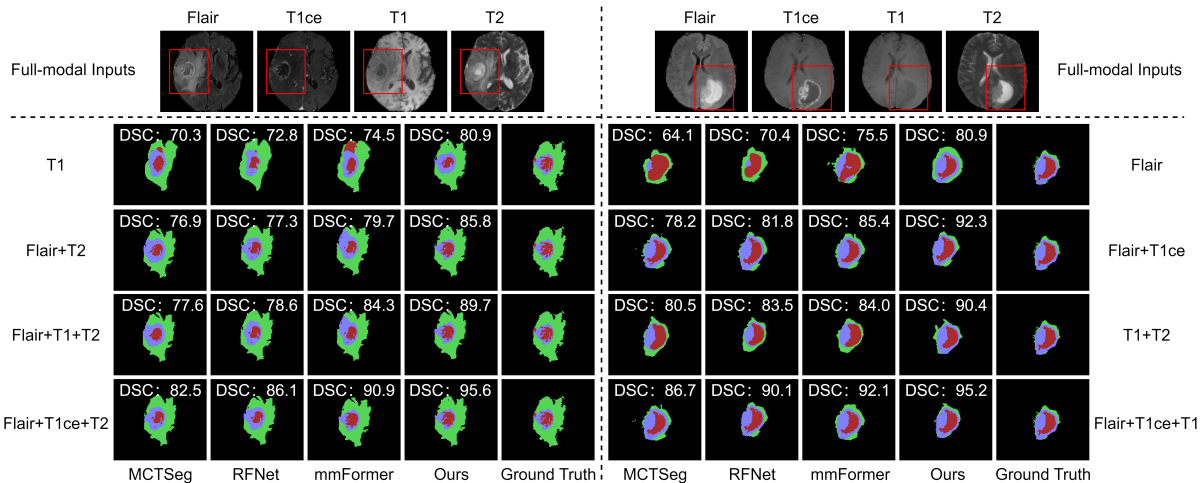


Figure 3: The first row shows full-modal inputs for two samples. Below are predicted segmentation masks for various missing modality settings. Green: peritumoral edema; blue: enhancing tumor; red: necrotic and non-enhancing tumor core.

image is available, due to the limited information from single modality. In contrast, our SMML maintains satisfactory performance under these conditions, illustrating the strength of our semantic-guided masked mutual learning in capturing robust and discriminative features for segmentation.

Methods	Avg DSC scores (%)			
	WT	TC	ET	Mean
MCTSeg	85.4	75.1	60.5	73.7
M3AE	86.9	79.1	61.7	75.9
U-Net-MFI	86.1	78.9	61.9	75.6
RFNet	86.3	78.0	61.4	75.2
mmFormer	86.5	78.3	65.1	76.6
SMU-Net	86.4	79.1	64.9	76.8
Ours	87.7	81.2	66.4	78.5

Table 3: Comparison results on the BraTs 2020 dataset.

Ablation Study

We evaluate the impact of each novel component in our SMML through ablation studies, incrementally integrating them into the baseline mmFormer model on the BraTs 2018 dataset. Table 4 illustrates the average DSC scores across various missing modality scenarios for each category, with an additional overall mean for direct comparison. As shown, the semantic-guided refinement network (SRN) achieves a 0.7% improvement over the baseline, confirming the benefit of auxiliary semantic information from SAM. Additionally, the dual-branch scheme alone surpasses the baseline by 0.8% in DSC, underscoring the efficacy of masked mutual learning. Based on the dual-branch scheme, the PBC, FRC, and SRN modules can further lead to notable improvements of 0.4%, 0.5% and 0.4%, respectively. Furthermore, the various combinations of different modules also lead to remarkable improvements. These highlight the indispensable role of these modules in learning robust and discriminative rep-

resentations for handling arbitrary missing modalities. Ultimately, integrating all proposed modules, the SMML framework attains a mean DSC score of 76.7% across the three categories, exceeding the baseline by 2.2%.

Dual-branch	PBC	FRC	SRN	DSC scores (%)			
				WT	TC	ET	Mean
				86.0	76.0	61.5	74.5
✓			✓	86.2	77.6	61.9	75.2
✓				86.3	77.3	62.4	75.3
✓	✓			86.8	78.0	62.3	75.7
✓		✓		86.5	77.6	63.2	75.8
✓			✓	86.5	77.4	63.2	75.7
✓	✓	✓		86.6	78.1	63.4	76.1
✓			✓	86.7	78.3	62.7	75.9
✓	✓	✓	✓	86.9	78.5	63.2	76.2
✓	✓	✓	✓	87.2	78.5	64.2	76.7

Table 4: Effectiveness of each SMML component.

Conclusion

We propose a novel Semantic-guided Masked Mutual Learning (SMML) method for brain tumor segmentation that flexibly addresses the challenges posed by diverse missing modality situations. Our SMML approach introduces a masked mutual learning scheme to emulate patient scenarios with varying missing modalities. We integrate Hierarchical Consistency Constraints (HCC) to transfer reliable knowledge and capture inter-sample and inter-class relational context in the latent feature space, enabling robust training of the SMML framework. Additionally, we incorporate a refinement network into each branch that leverages semantic priors from SAM, further enhancing the discriminative capability of our method without introducing additional computational burden during inference. Extensive experiments demonstrate that our SMML method significantly improves brain tumor segmentation performance under various missing modality settings.

Acknowledgements

This study was supported under the Key Research and Development Program of Zhejiang Province (Grant No. 2023C03192). It was also funded by the National Science Foundation of China (Grant No. 62201341).

References

- Azad, R.; Khosravi, N.; and Merhof, D. 2022. SMU-Net: Style matching U-Net for brain tumor segmentation with missing modalities. In *International Conference on Medical Imaging with Deep Learning*, 48–62. PMLR.
- Bakas, S.; Akbari, H.; Sotiras, A.; Bilello, M.; Rozycki, M.; Kirby, J. S.; Freymann, J. B.; Farahani, K.; and Davatzikos, C. 2017. Advancing the cancer genome atlas glioma MRI collections with expert segmentation labels and radiomic features. *Scientific data*, 4(1): 1–13.
- Ding, Y.; Yu, X.; and Yang, Y. 2021. RFNet: Region-aware fusion network for incomplete multi-modal brain tumor segmentation. In *Proceedings of the IEEE/CVF international conference on computer vision*, 3975–3984.
- Han, Z.; Zhang, C.; Fu, H.; and Zhou, J. T. 2020. Trusted multi-view classification. In *International Conference on Learning Representations*.
- Hinton, G.; Vinyals, O.; and Dean, J. 2015. Distilling the Knowledge in a Neural Network. *Computer Science*, 14(7): 38–39.
- Huang, Z.; and Wang, N. 2017. Like what you like: Knowledge distill via neuron selectivity transfer. *arXiv preprint arXiv:1707.01219*.
- Kang, M.; Ting, F. F.; Phan, R. C.-W.; Ge, Z.; and Ting, C.-M. 2024. A Multimodal Feature Distillation with CNN-Transformer Network for Brain Tumor Segmentation with Incomplete Modalities. *arXiv preprint arXiv:2404.14019*.
- Karimijafarbigloo, S.; Azad, R.; Kazerouni, A.; Ebadollahi, S.; and Merhof, D. 2023. MMCFormer: Missing Modality Compensation Transformer for Brain Tumor Segmentation. In *Medical Imaging with Deep Learning*.
- Kirillov, A.; Mintun, E.; Ravi, N.; Mao, H.; Rolland, C.; Gustafson, L.; Xiao, T.; Whitehead, S.; Berg, A. C.; Lo, W.-Y.; et al. 2023. Segment anything. In *Proceedings of the IEEE/CVF International Conference on Computer Vision*, 4015–4026.
- Li, X.; Lei, L.; Sun, Y.; and Kuang, G. 2021. Dynamic-hierarchical attention distillation with synergetic instance selection for land cover classification using missing heterogeneity images. *IEEE Transactions on Geoscience and Remote Sensing*, 60: 1–16.
- Liu, A.; Tan, Z.; Wan, J.; Liang, Y.; Lei, Z.; Guo, G.; and Li, S. Z. 2021. Face anti-spoofing via adversarial cross-modality translation. *IEEE Transactions on Information Forensics and Security*, 16: 2759–2772.
- Liu, H.; Wei, D.; Lu, D.; Sun, J.; Wang, L.; and Zheng, Y. 2023. M3AE: multimodal representation learning for brain tumor segmentation with missing modalities. In *Proceedings of the AAAI Conference on Artificial Intelligence*, 2, 1657–1665.
- Menze, B. H.; Jakab, A.; Bauer, S.; Kalpathy-Cramer, J.; Farahani, K.; Kirby, J.; Burren, Y.; Porz, N.; Slotboom, J.; Wiest, R.; et al. 2014. The multimodal brain tumor image segmentation benchmark (BRATS). *IEEE transactions on medical imaging*, 34(10): 1993–2024.
- Qiu, Y.; Chen, D.; Yao, H.; Xu, Y.; and Wang, Z. 2023. Scratch Each Other’s Back: Incomplete Multi-Modal Brain Tumor Segmentation via Category Aware Group Self-Support Learning. In *Proceedings of the IEEE/CVF International Conference on Computer Vision*, 21317–21326.
- Shaker, A. M.; Maaz, M.; Rasheed, H.; Khan, S.; Yang, M.-H.; and Khan, F. S. 2024. UNETR++: Delving into Efficient and Accurate 3D Medical Image Segmentation. *IEEE Transactions on Medical Imaging*, 1–1.
- Tung, F.; and Mori, G. 2019. Similarity-preserving knowledge distillation. In *Proceedings of the IEEE/CVF international conference on computer vision*, 1365–1374.
- Wang, H.; Guo, S.; Ye, J.; Deng, Z.; Cheng, J.; Li, T.; Chen, J.; Su, Y.; Huang, Z.; Shen, Y.; Fu, B.; Zhang, S.; He, J.; and Qiao, Y. 2023. SAM-Med3D. *arXiv:2310.15161*.
- Wang, H.; Zhang, J.; Chen, Y.; Ma, C.; Avery, J.; Hull, L.; and Carneiro, G. 2022. Uncertainty-aware multi-modal learning via cross-modal random network prediction. In *European Conference on Computer Vision*, 200–217. Springer.
- Wei, S.; Luo, C.; and Luo, Y. 2023. MMANet: Margin-aware distillation and modality-aware regularization for incomplete multimodal learning. In *Proceedings of the IEEE/CVF Conference on Computer Vision and Pattern Recognition*, 20039–20049.
- Wu, L.; Lin, H.; Huang, Y.; Fan, T.; and Li, S. Z. 2023. Extracting low-/high-frequency knowledge from graph neural networks and injecting it into mlps: An effective gnn-to-mlp distillation framework. In *Proceedings of the AAAI Conference on Artificial Intelligence*, 9, 10351–10360.
- Yan, J.; Chen, S.; Zhang, Y.; and Li, X. 2020. Neural architecture search for compressed sensing magnetic resonance image reconstruction. *Computerized Medical Imaging and Graphics*, 85: 101784.
- Yang, C.; Zhou, H.; An, Z.; Jiang, X.; Xu, Y.; and Zhang, Q. 2022. Cross-image relational knowledge distillation for semantic segmentation. In *Proceedings of the IEEE/CVF Conference on Computer Vision and Pattern Recognition*, 12319–12328.
- Zagoruyko, S.; and Komodakis, N. 2017. Paying More Attention to Attention: Improving the Performance of Convolutional Neural Networks via Attention Transfer. In *The 5th International Conference on Learning Representations*.
- Zhang, Y.; He, N.; Yang, J.; Li, Y.; Wei, D.; Huang, Y.; Zhang, Y.; He, Z.; and Zheng, Y. 2022. mmformer: Multimodal medical transformer for incomplete multimodal learning of brain tumor segmentation. In *International Conference on Medical Image Computing and Computer-Assisted Intervention*, 107–117.
- Zhao, Z.; Yang, H.; and Sun, J. 2022. Modality-adaptive feature interaction for brain tumor segmentation with missing modalities. In *International Conference on Medical Image*

Computing and Computer-Assisted Intervention, 183–192. Springer.

Zhou, H.-Y.; Guo, J.; Zhang, Y.; Han, X.; Yu, L.; Wang, L.; and Yu, Y. 2023. nnFormer: Volumetric Medical Image Segmentation via a 3D Transformer. *IEEE Transactions on Image Processing*, 32: 4036–4045.